scientific reports

Check for updates

OPEN

Single-cell sequencing and transcriptomic data reveal that P65 activation significantly promotes microglia-mediated neuroinflammation after ischemic stroke

Ruiyu Wang[1,4], Yilun Qian[1,4], Xinchen Zhou[2,4], Hang Xu[3], Yu Wang[1], Yao Geng[1]✉, Tianshu Wang[1]✉ & Binxiu Sha[1]✉

The pathophysiological mechanisms underlying cerebral ischemia-reperfusion (I/R) injury are highly complex. Previous studies have indicated phenotypic changes in various cell types following stroke but have failed to identify the key regulatory genes and cell subtypes associated with the disease. The study utilized five datasets: GSE227651, GSE104036, GSE116878, GSE249957, and GSE22255. The Seurat pipeline was employed for standard quality control and single-cell data analysis. Monocle2 and CytoTRACE were used for trajectory analysis, while Mfuzz was applied to identify time-series gene expression patterns. Middle cerebral artery occlusion (MCAO) mice served as the animal model for cerebral I/R injury, and oxygen-glucose deprivation/reoxygenation (OGD/R)-treated BV2 cells were used to simulate microglial phenotypic changes following ischemia-reperfusion. qPCR, Western blotting, and immunofluorescence staining were used to detect key gene and protein alterations. P65 was identified as a key transcription factor driving inflammatory responses and transcriptional changes following ischemic stroke. Two microglial subtypes, Cx3cr1 + and Cdk1+, were identified, with their proportions significantly increasing on days 1 and 3 after MCAO. Increased levels of inflammation, neuronal apoptosis, and P65 phosphorylation in microglia were observed in both the MCAO animal model and OGD/R cell model. Notably, inhibition of P65 phosphorylation effectively suppressed the progression of inflammation during cerebral I/R injury. We identified microglial subtypes associated with inflammatory responses following cerebral ischemia-reperfusion injury, with their proportions increasing post-injury. P65 was confirmed as a critical regulator of the inflammatory response, contributing to neuronal protection and the restoration of neurological function.

Keywords Middle cerebral artery occlusion, Stroke, Single cell, Transcription factor

Abbreviations

I/R	Ischemia-reperfusion
MCAO	Middle cerebral artery occlusion
OGD/R	Oxygen-glucose deprivation/reoxygenation
GEO	Gene Expression Omnibus
tMCAO	Transient middle cerebral artery occlusion
PBMC	Peripheral blood mononuclear cells
DEGs	Differentially expressed genes

[1]The First Affiliated Hospital With Nanjing Medical University, Nanjing, Jiangsu Province, People's Republic of China. [2]School of Nursing and Rehabilitation, Nantong University, Nantong, Jiangsu Province, People's Republic of China. [3]Nanjing Medical University, Nanjing, Jiangsu Province, People's Republic of China. [4]Ruiyu Wang, Yilun Qian and Xinchen Zhou contributed equally to this work. ✉email: gengyao19970821@163.com; wts15951928785@gmail.com; njsbx2011@163.com

TFs Transcription factors

Cerebral ischemia-reperfusion (I/R) injury is a multifaceted pathological condition that results in significant neurological impairments[1]. The underlying mechanisms involve a cascade of complex biological processes, including inflammation, neuronal apoptosis, and tissue remodeling[2]. Recent advancements in transcriptomics, particularly single-cell RNA sequencing (scRNA-seq), have offered unprecedented opportunities to explore cellular heterogeneity and dynamic molecular changes following ischemic stroke[3]. However, identifying key regulatory genes and specific cell subtypes involved in neuroinflammation remains a significant challenge.

Microglia, the resident immune cells of the central nervous system, play a pivotal role in mediating inflammatory responses during cerebral I/R injury[4]. Their activation is accompanied by extensive transcriptional reprogramming, which contributes to both neuroprotection and neurodegeneration[5–7]. Among the transcriptional regulators implicated in microglial activation, the NF-κB signaling pathway has garnered particular attention due to its central role in driving proinflammatory responses[8]. Specifically, P65 (RELA), a key component of the NF-κB pathway, has been shown to influence inflammatory cascades and neuronal survival during ischemic events[9].

This study employs an integrative approach combining single-cell transcriptomic analysis with in vivo and in vitro experiments to elucidate the role of P65 in microglial activation and its downstream effects on neuroinflammation and neuronal apoptosis. By leveraging datasets such as GSE227651, GSE104036, GSE116878, GSE249957 and GSE22255 we systematically characterized the transcriptional landscape of microglia and identified key subtypes involved in inflammatory responses post-stroke. These findings were further validated in middle cerebral artery occlusion (MCAO) animal models and oxygen-glucose deprivation/reoxygenation (OGD/R)-treated BV2 cells. Our results highlight the critical role of P65 activation in amplifying microglia-mediated neuroinflammation, which exacerbates neuronal apoptosis and impairs functional recovery.

Results

Single-cell landscape of mouse brains at different time points Post-MCAO

Cerebral ischemia-reperfusion involves complex pathophysiological mechanisms, with phenotypic changes occurring in different cell types at specific time points[10]. After data curation, single-cell sequencing analysis of the ipsilateral brain hemispheres from sham-operated mice and mice at 1, 3, and 7 days post-MCAO revealed the presence of 10 major cell populations in the mouse brain: Endothelial (Cldn5+, Flt1+), Oligodendrocytes (Olig1+, Mobp+), Pericytes (Vtn+, Pdgfrb+), VSMCs (Acta2+, Myh11+), Microglia (C1qa+, C1qb+), Neurons (Meg3+, Rtn1+), Epithelial cells (Krt18+), Astrocytes (Aqp4+, Gfap+), OPCs (Pdgfra+, Vcan+), and Fibroblasts (Dcn+, F3+). Among these, the proportions of Microglia and Astrocytes significantly increased following stroke, while the proportion of Neurons significantly decreased at day 3 post-stroke (Fig. 1A–C).

KEGG enrichment analysis of genes significantly upregulated at different time points post-MCAO revealed activation of the HIF-1 signaling pathway, cytokine-cytokine receptor interaction, NF-kappa B signaling pathway, phagosome formation, efferocytosis, and apoptosis (Fig. 1D,E) (www.kegg.jp/kegg/kegg1.html). Similarly, GO enrichment analysis indicated significant activation of terms such as cytokine binding, immune receptor activity, and transcription coregulator activity (Fig. 1F), suggesting heightened inflammatory activation, increased cytokine release, and enhanced immune cell phagocytic activity after MCAO[11,12]. Scoring of significantly activated terms across all cell populations revealed that Microglia exhibited the highest scores, indicating that Microglia play a central role in inflammatory responses and immune regulation following MCAO (Fig. 1G–I).

Transcriptome sequencing analysis of mouse brains at different time points post-MCAO

To further investigate the transcriptional changes and dynamic expression patterns of genes in the ipsilateral brain hemisphere at different time points after MCAO, two datasets of mRNA sequencing data from MCAO-operated mice were analyzed. Compared to the sham group, analysis of the GSE104036 dataset revealed 1204 significantly upregulated genes and 853 significantly downregulated genes at 3 h post-MCAO; 2720 upregulated and 1964 downregulated genes at 6 h; 2842 upregulated and 2469 downregulated genes at 12 h; and 3,130 upregulated and 3149 downregulated genes at 24 h (Fig. 2A). Similarly, analysis of the GSE116878 dataset revealed 432 significantly upregulated genes and 524 downregulated genes immediately after MCAO; 1477 upregulated and 717 downregulated genes at 3 h; 1489 upregulated and 772 downregulated genes at 12 h; 1972 upregulated and 1571 downregulated genes at 24 h; and 1810 upregulated and 840 downregulated genes at 72 h (Fig. 2B).

Dynamic gene expression patterns after MCAO were explored using Mfuzz. Based on the optimal number of clusters, gene expression trends were categorized into four distinct clusters (Fig. 2C,D). In the GSE104036 dataset, cluster analysis revealed significant enrichment at 6 h post-MCAO in processes such as "pattern specification process", "embryonic organ morphogenesis", and "cell fate commitment" indicating the initiation of brain tissue repair and structural remodeling. At 12 h, processes such as "mRNA processing", "RNA splicing" and "ncRNA processing" were significantly enriched, reflecting substantial changes in gene expression regulation and protein homeostasis, likely aimed at repairing damaged brain tissue, regulating inflammation, and maintaining cellular function. At 24 h, processes such as "regulation of innate immune response", "regulation of immune effector process", and "cytokine-mediated signaling pathway" were enriched, indicating the activation of nonspecific immune responses, complement system activation, and enhanced phagocytosis to clear necrotic cells and debris, thereby protecting neurons and promoting tissue repair (Fig. 2C)[13,14]. Similarly, four distinct dynamic gene expression patterns were identified in the GSE116878 dataset. Significant changes in gene regulation and protein homeostasis were observed at 3, 12, and 24 h post-MCAO, while robust activation of the immune system and inflammatory responses was evident at 72 h (Fig. 2D).

KEGG and GO enrichment analyses were performed on significantly upregulated and downregulated genes at different time points post-MCAO. KEGG analysis revealed significant activation of pathways such as "TNF

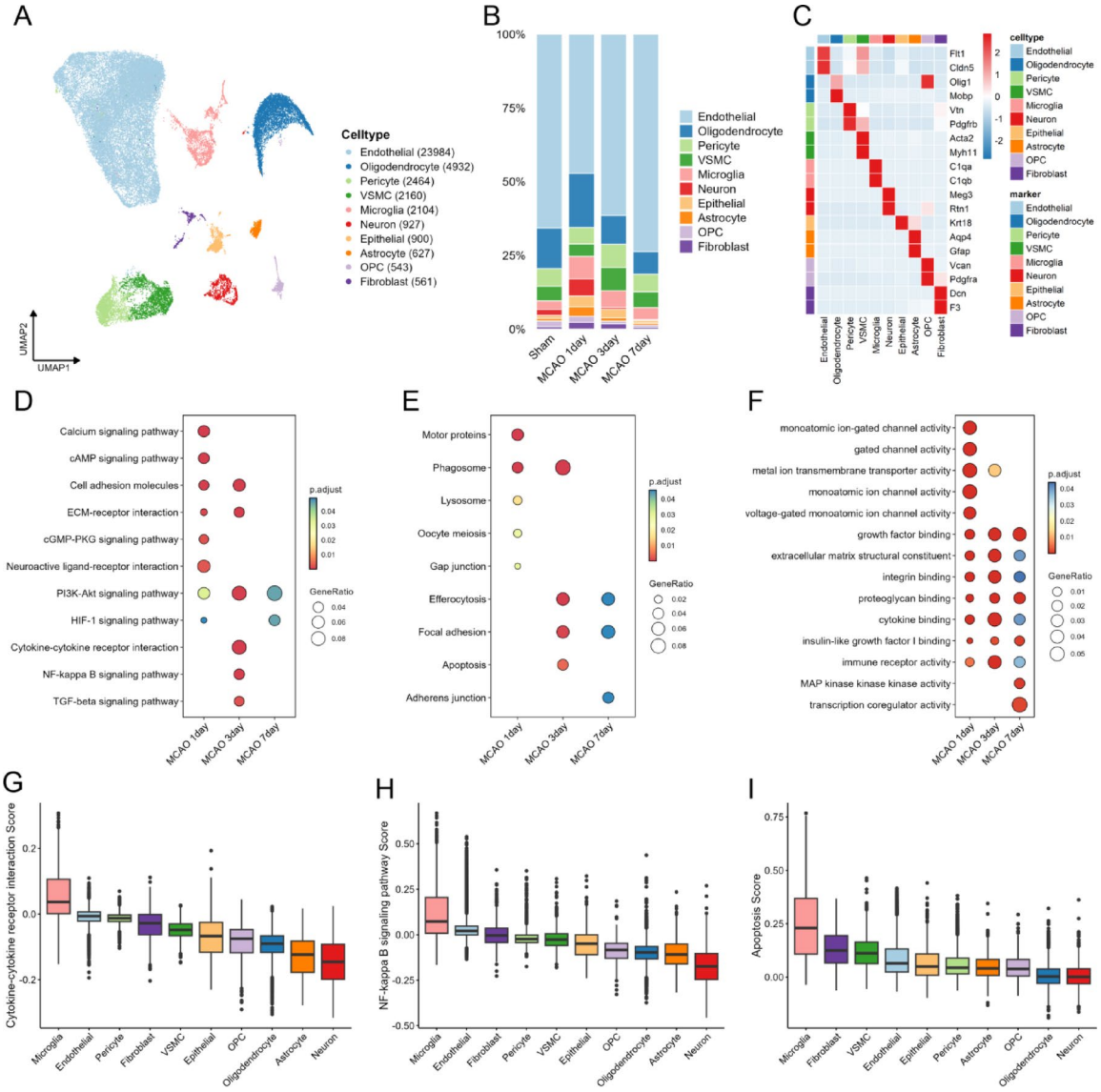

Fig. 1. Cellular atlas of the ipsilateral brain hemisphere of mice at different time points following MCAO. (**A**) UMAP dimensionality reduction plot. (**B**) Proportions of cell types at different time points post-MCAO. (**C**) Heatmap of marker genes used for cell annotation. (**D**,**E**) KEGG enrichment analysis of differentially expressed genes (DEGs) at various time points post-MCAO. (**F**) GO enrichment analysis of DEGs at different time points post-MCAO. (**G**–**I**) Boxplots of cell scores ranked from high to low at different time points post-MCAO.

signaling pathway", "NF-kappa B signaling pathway" and "IL-17 signaling pathway" across different stages of MCAO, while pathways related to "oxidative phosphorylation", "pathways of neurodegeneration–multiple diseases" and "synaptic vesicle cycle" were significantly suppressed. These findings indicate prominent immune cell infiltration, inflammation, and neuronal dysfunction following MCAO (Fig. 2E–H). GO enrichment results further demonstrated significant activation of terms such as "cytokine activity", "cytokine receptor binding", "transcription factor binding" and "immune receptor activity" while terms such as "sodium ion transmembrane transporter activity", "metal ion transmembrane transporter activity" and "gated channel activity" were significantly suppressed. These findings suggest pronounced changes in gene regulation, inflammation, impaired neuronal signaling, and ion homeostasis dysregulation after MCAO (Fig. 2I–L).

Identification of key transcription factors associated with inflammatory activation

Transcription factors (TFs) are proteins that bind to specific DNA sequences, such as promoters and enhancers, to regulate gene transcription, thereby influencing a wide range of biological processes[15]. Transcription factors can exacerbate inflammatory damage or participate in anti-inflammatory repair mechanisms[16]. Based on the previous analytical results, to identify key transcription factors associated with inflammation activation and dynamic gene expression changes, transcription factor activities at different time points post-MCAO were scored using the decoupleR package. The GSE104036 dataset revealed that transcription factors related to the

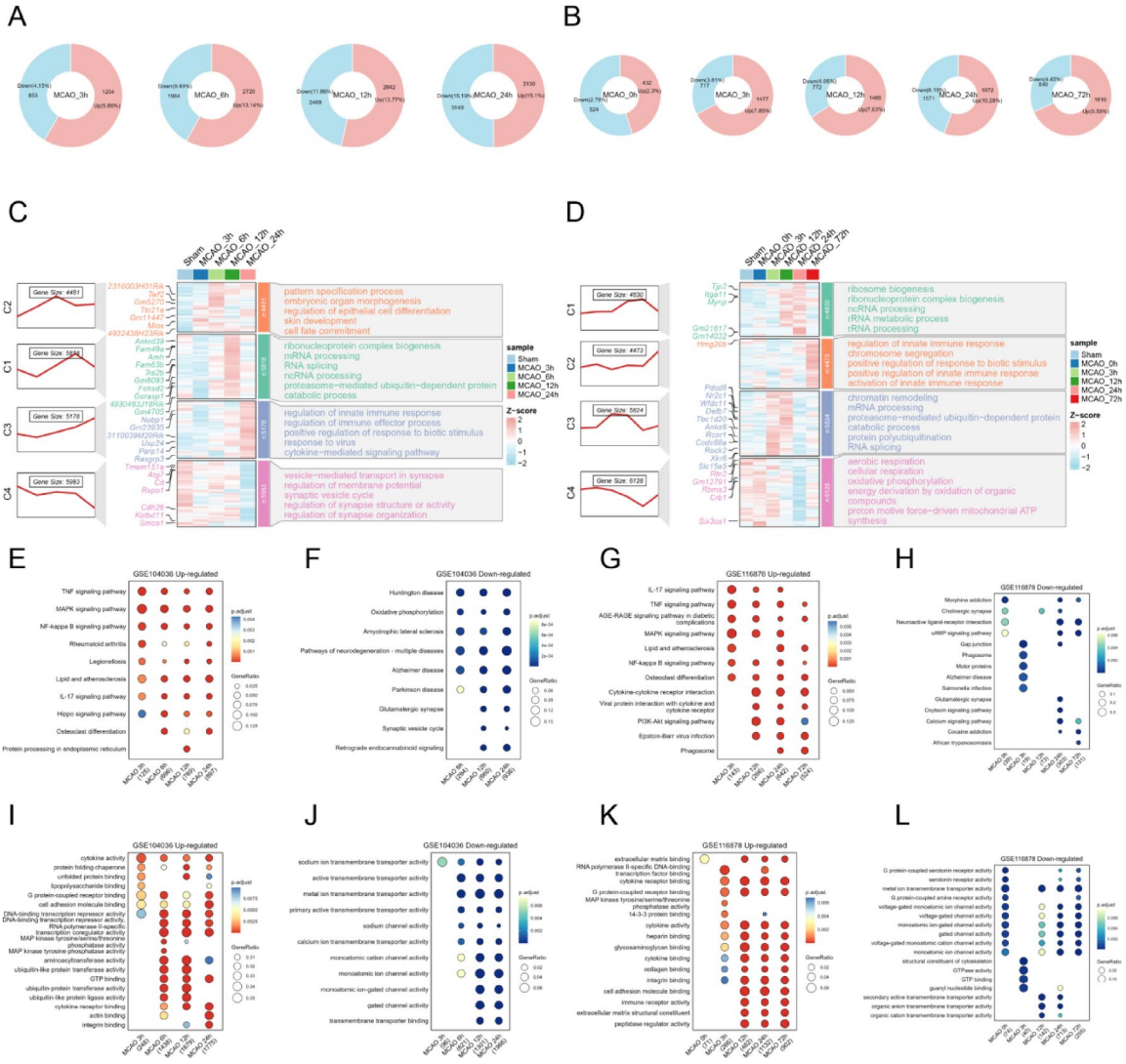

Fig. 2. Transcriptome sequencing analysis of mouse brains at different time points following MCAO. (A-B) Number of differentially expressed genes (DEGs) at various time points post-MCAO: (**A**) GSE104036, (**B**) GSE116878. (**C**,**D**) Mfuzz analysis revealing four dynamic gene expression patterns over time post-MCAO: (**C**) GSE104036, (**D**) GSE116878. (**E**,**F**) KEGG enrichment analysis of significantly upregulated and downregulated genes at different time points post-MCAO: (**E**) GSE104036, (**F**) GSE116878. (**G**,**H**) GO enrichment analysis of significantly upregulated and downregulated genes at different time points post-MCAO: (**G**) GSE104036, (**H**) GSE116878.

NF-κB signaling pathway, including Rela (P65) and Nfkb1 (p50)[17], exhibited high activity scores at 3, 6, 12, and 24 h post-MCAO (Fig. 3A–D). Similarly, the GSE116878 dataset al.so showed high activity scores for Rela (P65) and Nfkb1 (p50) at various post-MCAO time points (Fig. 3E–H). Scoring across datasets further demonstrated elevated activities of Rela (P65) and Nfkb1 (p50) in Microglia and Fibroblasts (Fig. 3I–J).

To validate the reliability and generalizability of these results, mRNA sequencing data from BV2 microglial cells subjected to oxygen-glucose deprivation/reoxygenation (OGD/R) were used to simulate transcriptional changes in microglia during ischemic stroke (Fig. 4A). KEGG enrichment analysis revealed significant activation of pathways such as Apoptosis, Toll-like receptor signaling, and TNF signaling, with a notable upregulation of Rela (Fig. 4B). Similarly, GO enrichment analysis indicated substantial changes in gene regulation and protein homeostasis in microglia following OGD/R treatment, alongside enhanced transcription factor activity (Fig. 4C). Further validation was conducted using microarray data from human ischemic stroke patients (Fig. 4D). KEGG enrichment analysis demonstrated significant activation of the NF-κB signaling pathway, IL-7 signaling pathway, and TNF signaling pathway, with RELA significantly upregulated (Fig. 4E). GO analysis also indicated increased immune cell infiltration and enhanced transcription factor activity (Fig. 4F). Correlation analyses of P65-regulated gene networks and GSVA scores for the NF-κB signaling pathway across datasets revealed a significant positive correlation between P65 activity and NF-κB signaling pathway activity. Moreover, mice subjected to

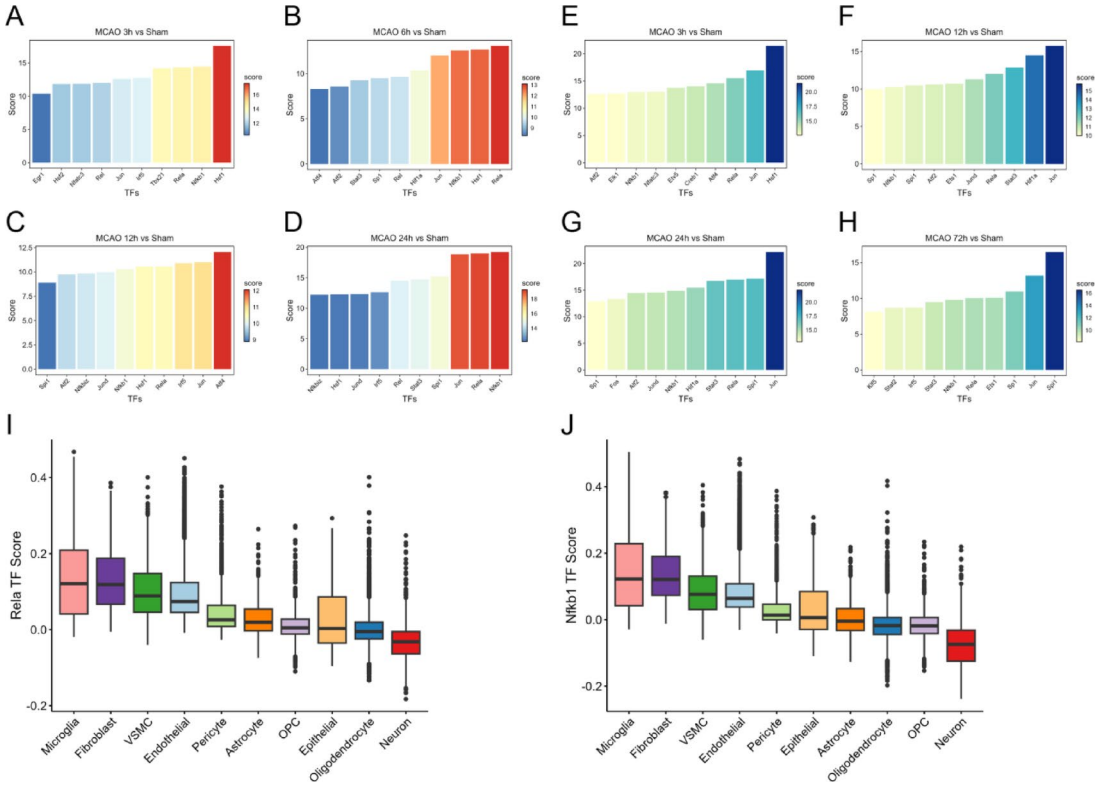

Fig. 3. Identification of key transcription factors associated with inflammatory activation. (**A**–**D**) Bar plots of transcription factor activity scores at different time points post-MCAO in the GSE104036 dataset. (**E**–**H**) Bar plots of transcription factor activity scores at different time points post-MCAO in the GSE116878 dataset. (**I**–**J**) Boxplots of cell scores for key transcription factors in the NF-κB signaling pathway, ranked in descending order of score.

MCAO, BV2 cells treated with OGD/R, and human blood samples from ischemic stroke patients exhibited higher levels of P65 activity and NF-κB signaling pathway activation (Fig. 4G–J).

Microglial subsets and trajectory analysis

To investigate the key microglial subpopulations involved in the inflammatory response and the regulatory role of the Rela transcriptional network in microglial activity following MCAO, we conducted a detailed analysis of microglial subpopulations. Microglia were classified into nine subpopulations based on marker expression: Cx3cr1+, Flt1+, Ms4a7+, Cdk1+, Ccr2+, Gpr37+, Pdgfrb+, Cd79a+, and Hba-a1+. Among these, the proportions of Cx3cr1 + Microglia and Cdk1 + Microglia were significantly increased on days 1 and 3 post-stroke (Fig. 5A–C). Trajectory analysis combined with CytoTRACE inferred the starting point of the trajectory as State 3, with one branching point and three distinct states (Fig. 5D–G). State 1 exhibited the highest P65 activity scores, with Cx3cr1 + Microglia and Cdk1 + Microglia being predominant within this state (Fig. 5H,I). KEGG enrichment analysis of genes driving the differentiation of microglia from the branching point toward State 1 revealed significant involvement in the NF-κB signaling pathway, TNF signaling pathway, Toll-like receptor signaling pathway, and Apoptosis (Fig. 5J). These findings suggest that Cx3cr1 + Microglia and Cdk1 + Microglia are the primary microglial subpopulations contributing to inflammatory activation following MCAO and are regulated by the Rela transcriptional network.

Inflammatory factors are up-regulated in tMCAO mice, and microglia activation is accompanied by increased phosphorylation of P65

To elucidate the mechanism of P65 regulation, we constructed the tMCAO mouse model. The tMCAO group underwent transient middle cerebral artery occlusion (tMCAO) surgery to prepare the I/R brain injury model. Figure 6A presents a schematic diagram of the animal experimental workflow. The sham group underwent the same procedure but without monofilament insertion. tMCAO mice had reduced scores in the neurological function assessment and balance beam test (Fig. 6B,C), regional cerebral blood flow measurements showed decreased regional cerebral blood flow in the tMCAO group (Fig. 6D,E), and TTC staining showed significant infarct localized in the tMCAO group (Fig. 6F,G). Phosphorylation of P65 was significantly increased in the infarcted area of tMCAO mice (Fig. 6H–K), along with a significant increase in proinflammatory markers, including IL-6, TNF-α, and IL-1β (Fig. 6L–N).

Immunofluorescence staining was used to quantify the number of neurons (Neun) and microglia (Iba1) and the expression of P-P65. tMCAO mice had a significant reduction in the number of neurons in the infarct area

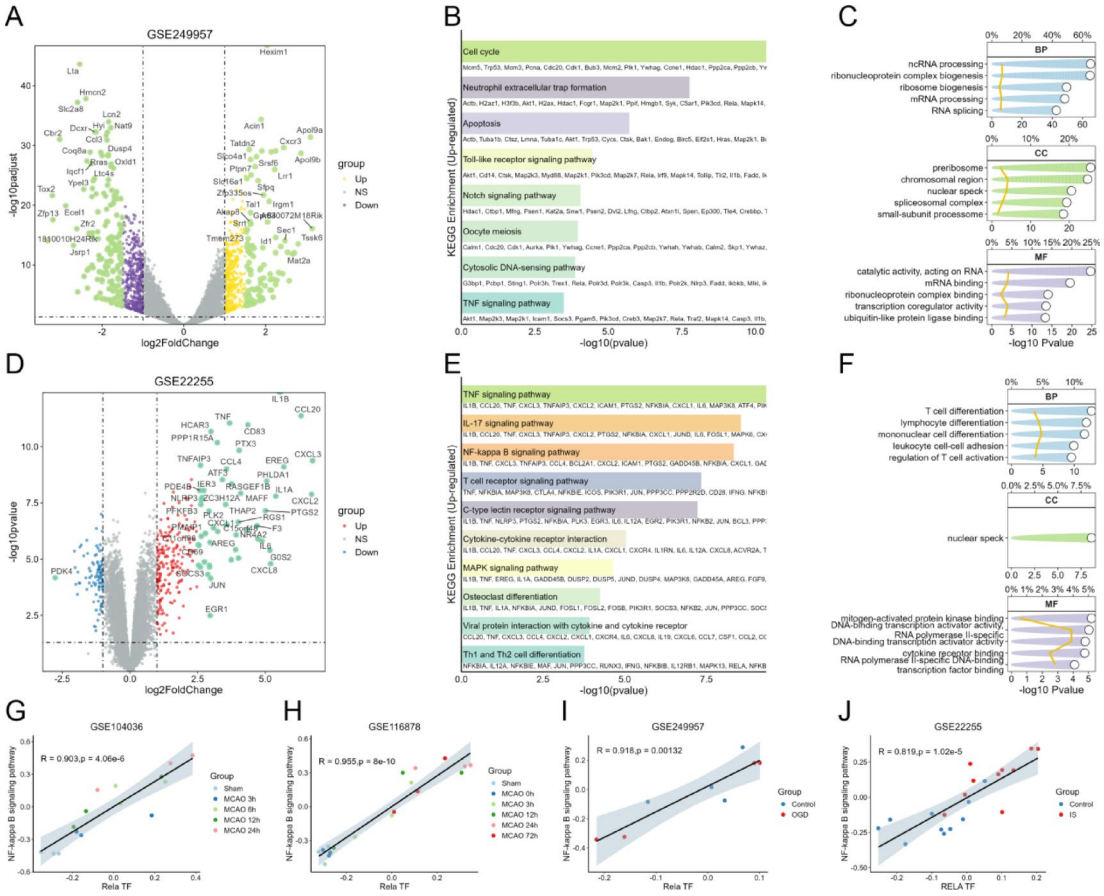

Fig. 4. Validation of key transcription factors involved in inflammatory activation after ischemic stroke. (**A**) Volcano plot of differentially expressed genes (DEGs) between OGD/R-treated BV2 cells and control group. (**B**) KEGG enrichment analysis of significantly upregulated genes in BV2 cells. (**C**) GO enrichment analysis of significantly upregulated genes in BV2 cells. (**D**) Volcano plot of differentially expressed genes in human ischemic stroke blood samples. (**E**) KEGG enrichment analysis of significantly upregulated genes in human ischemic stroke blood. (**F**) GO enrichment analysis of significantly upregulated genes in human ischemic stroke blood. (**G**–**J**) Correlation analysis of GSVA scores for the NF-κB signaling pathway and P65 transcription factor.

and a significant increase in the number of IBA1 + microglia, accompanied by an increase in P65 phosphorylation (Fig. 7A–D). Cytoskeleton analysis of IBA1 + microglia showed that the cell body of microglia in tMCAO mice was significantly larger and the average branch length was shortened (Fig. 7A,E,F), indicating the presence of activation of microglia in tMCAO mice. Immunofluorescence co-localization analysis further showed that the proportion of IBA1 + P-P65 + microglia was significantly increased in tMCAO mice, and P65 phosphorylation was activated in microglia of stroke mice (Fig. 7G,H).

Inhibition of P65 phosphorylation can reduce the levels of inflammatory factors in microglia and provide neuroprotection

To explore the differences in microglia neuroinflammation between tMCAO mice and sham mice, and the role of P65 in this process, we treated BV2 cells with OGD/R to simulate the ischemia-hypoxia state. The Fig. 8A illustrates a schematic representation of the cell experiment. BV2 cells and conditioned medium were collected to detect the phosphorylation level of P65 and the expression of cytokines in BV2 cells. The conditioned medium of BV2 cells was co-cultured with SH-SY5Y cells for 24 h to detect neuronal activity. The results showed that the expression of proinflammatory cytokines IL-6, TNF-α, and IL-1β was increased in BV2 cells treated with OGD/R. However, treatment with JSH23, an inhibitor of P65 phosphorylation, significantly reduced this proinflammatory response (Fig. 8F–H). P-P65 expression was increased in BV2 cells treated with OGD/R, but P65 phosphorylation was decreased in cells co-treated with OGD/R and JSH23 (Fig. 8B–E). In addition, SH-SY5Y cells co-cultured with conditioned medium from OGD/R-treated microglia showed an increased proportion of apoptosis, which was significantly attenuated by the addition of JSH23 (Fig. 8I,J). A schematic of the study is shown in (Fig. 8K).

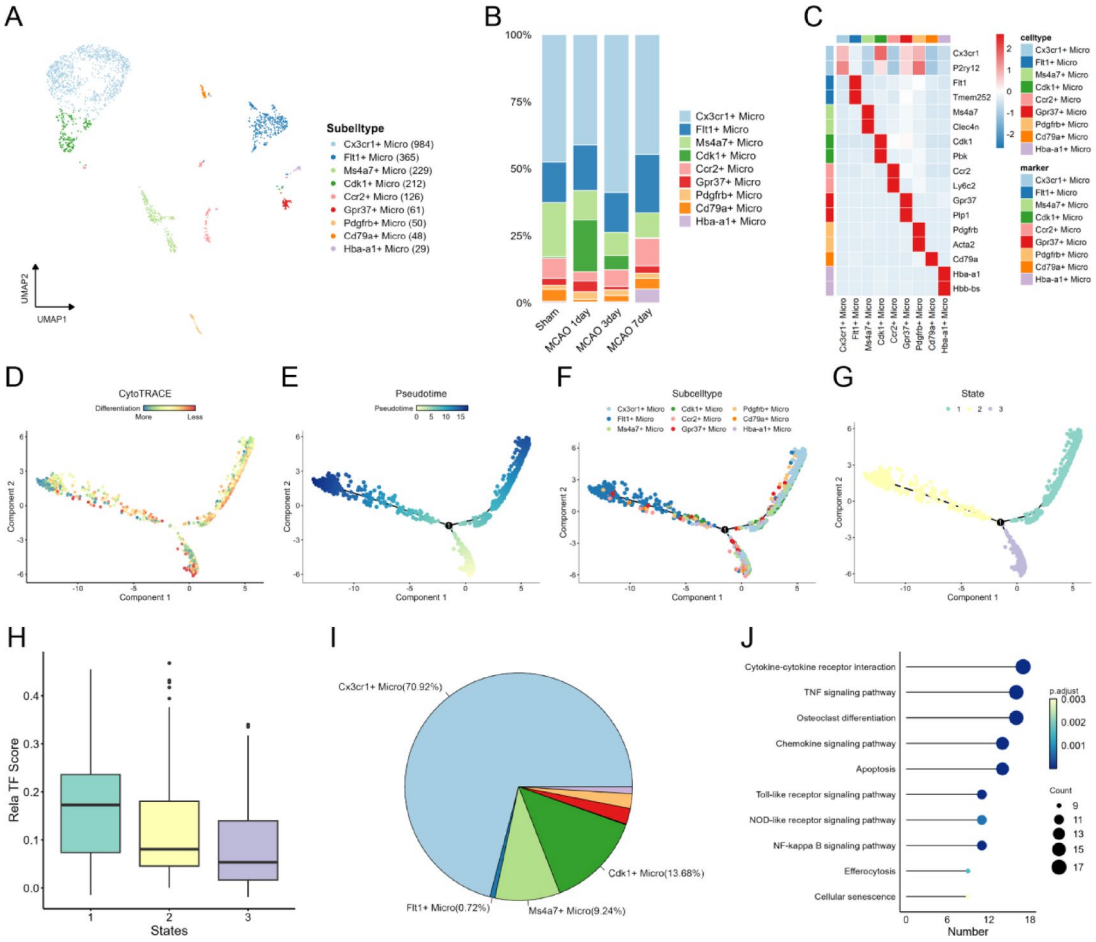

Fig. 5. Microglial subsets and trajectory analysis. (**A**) UMAP plot of microglial subsets. (**B**) Proportions of microglial subsets at different time points post-MCAO. (**C**) Heatmap of marker genes used for microglial subset identification. (**D**) CytoTRACE inference of the trajectory origin. (**E**) Pseudotime trajectory of microglial subsets. (**F**) Trajectory of microglial cell subsets. (**G**) Different states of microglial differentiation. (**H**,**I**) P65 scores in microglial cells at different states, along with the proportion of microglial subsets in state 1. (**J**) KEGG enrichment analysis of genes driving the differentiation of microglial cells from branch point 1 to state 1.

Discussion

This study comprehensively analyzes the transcriptional dynamics and functional roles of microglia in ischemic stroke, focusing on the NF-κB signaling pathway and its key regulator, P65. By integrating single-cell transcriptomics, bioinformatics, and experimental validation, this study reveals novel mechanisms of microglial activation and its contribution to post-stroke neuroinflammation.

In comparison to previous studies, which broadly described the role of microglia in post-stroke inflammation[18,19], this study refines this understanding by identifying specific microglial subtypes involved in the process. For the first time, we identified the significant activation of Cx3cr1 + and Cdk1 + microglial subtypes following ischemic stroke, providing new perspectives on microglial heterogeneity and their functional roles.

The NF-κB signaling pathway is well-established as a driver of neuroinflammation[20,21], but the specific role of P65 (Rela) remains unclear. Our findings reveal that P65 phosphorylation acts as a molecular switch promoting the production of pro-inflammatory cytokines such as IL-6, TNF-α, and IL-1β, thereby exacerbating neuronal apoptosis. These results extend the understanding of transcriptional regulators in microglial activation and underscore the central role of P65 in regulating inflammatory responses in specific microglial subtypes[22]. Additionally, bioinformatics analysis using datasets such as GSE227651 revealed dynamic changes in inflammatory pathways within the microglial transcriptional landscape after stroke.

Using the MCAO model, we validated these findings in vivo, demonstrating that ischemic stroke induces robust microglial activation characterized by increased P65 phosphorylation and elevated expression of pro-inflammatory cytokines. While prior studies highlighted the critical role of microglia in the progression of ischemic damage[23], this study goes further by providing detailed analyses of specific transcriptional regulators and microglial subtypes driving these effects. Furthermore, we showed that inhibiting P65 phosphorylation with JSH23 significantly reduced inflammation and neuronal apoptosis, consistent with previous research on the therapeutic potential of transcription factor inhibition[24].

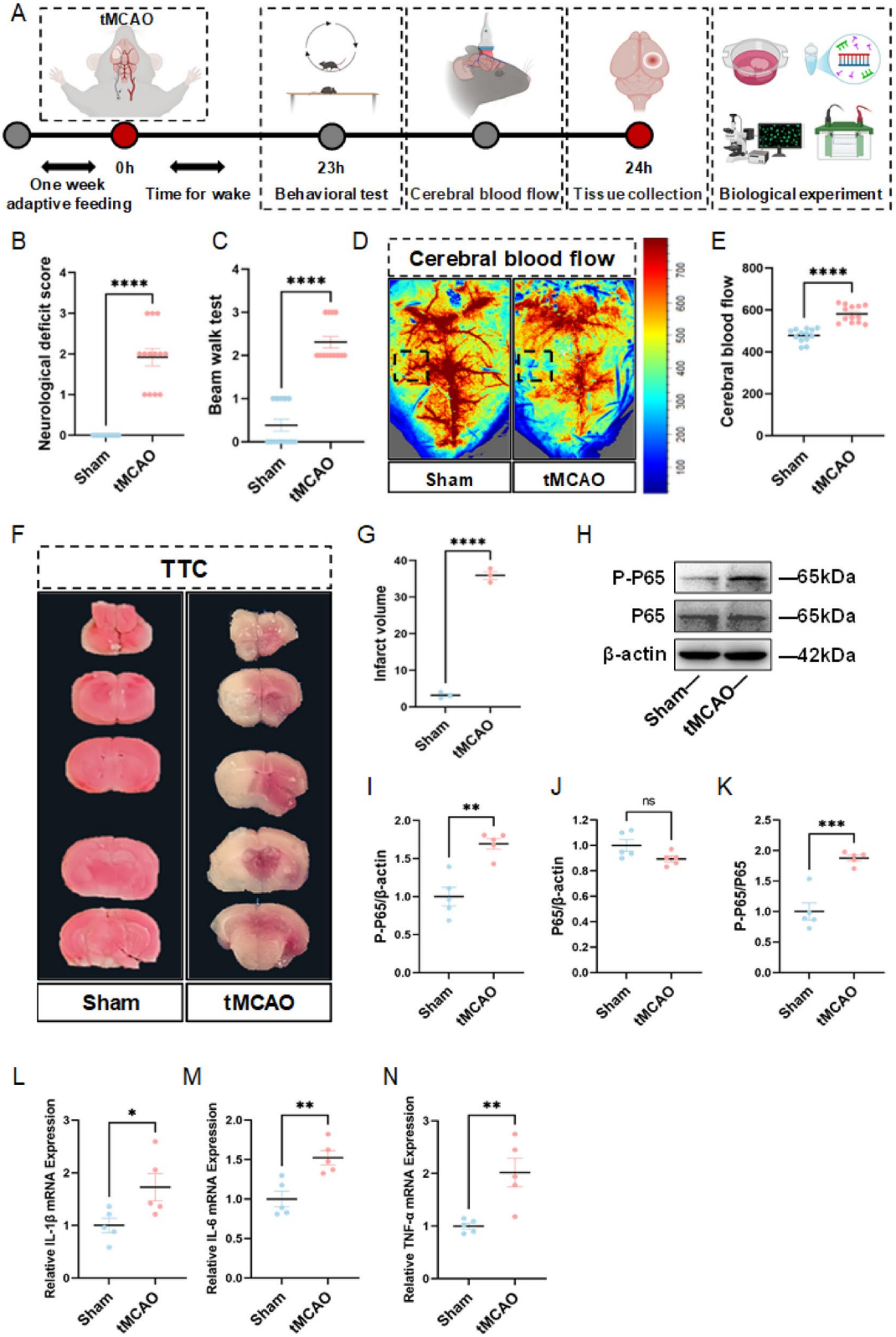

In vitro experiments using OGD/R-treated BV2 cells provided further mechanistic insights. These experiments demonstrated that OGD/R induces P65 phosphorylation and pro-inflammatory cytokine production, both of which were significantly mitigated by JSH23 treatment. While prior studies explored the effects of OGD/R on microglial activation[25], this study uniquely elucidates the specific regulatory role of P65 in this process and its downstream impact on neuronal survival. Co-culture experiments further highlighted the neuroprotective effects of inhibiting P65 phosphorylation, as conditioned media from treated BV2 cells significantly improved SH-SY5Y cell viability. This aligns with earlier findings that targeting microglial-mediated inflammation can reduce neuronal damage[26].

◀**Fig. 6**. Inflammatory factors are up-regulated in the infarct area of tMCAO mice, accompanied by increased phosphorylation of P65. (**A**) Flow chart of the experiment: After one week of adaptive feeding, mice in the tMCAO group were subjected to transient middle cerebral artery occlusion surgery, and those in the Sham group were subjected to the same surgery but only blood vessels and nerves were exposed without ligation and insertion of emboli. Neurological function and cerebral blood flow were assessed after the mice were confirmed to be fully awake, and euthanasia and tissue collection were completed within 24 h after surgery. (**B**,**C**) Behavior test: Neurological deficit score and Beam walk test ($n = 13$). (**D**,**E**) Cerebral blood flow imaging, quantitative statistical analysis of mean cerebral blood flow ($n = 13$). (**F**,**G**) Representative images for infarct volume assessment (TTC staining) and statistical analysis ($n = 3$). (**H**–**K**) Representative bands of Western blot and statistical analysis for P-P65, P65, and β-actin ($n = 5$). (**L**–**N**) qRT-PCR statistical analysis of IL-1β, IL-6 and TNF-α ($n = 5$). Data are Mean ± SEM. $*p < 0.05$, $**p < 0.01$, $***p < 0.001$, and $****p < 0.0001$.

Despite these advancements, this study has certain limitations. First, while we elucidated the early role of P65 phosphorylation in neuroinflammation, the long-term effects of its inhibition on tissue repair and functional recovery remain unexplored. Second, although human transcriptomic datasets were analyzed, experimental validation was primarily conducted in murine models and BV2 cells, limiting the direct applicability of findings to stroke patients. Third, interactions between the NF-κB pathway and other signaling cascades, such as MAPK and JAK-STAT, require further investigation to comprehensively understand the complexity of post-stroke inflammation. Finally, while specific microglial subtypes were identified and characterized, their functional roles, such as contributions to phagocytosis and cytokine secretion, warrant further validation.

Conclusion

This study integrates single-cell transcriptomics, bioinformatics, and experimental validation to elucidate the role of P65-mediated microglial activation in ischemic stroke. We identified Cx3cr1 + and Cdk1 + microglial subtypes that play critical roles in post-stroke inflammation and demonstrated that P65 phosphorylation serves as a key regulatory mechanism driving the production of pro-inflammatory cytokines and neuronal apoptosis. Using MCAO models and OGD/R-treated BV2 cells, we validated the therapeutic potential of P65 inhibition in mitigating neuroinflammation and promoting neuronal survival. While our findings highlight the critical role of P65 in neuroinflammation, further studies are needed to evaluate the long-term effects of its inhibition, explore interactions with other signaling pathways, and validate the findings in human models.

Materials and methods

Data collection

Datasets GSE227651[27], GSE104036, GSE116878[28], GSE249957[29], and GSE22255[30] were selected from the Gene Expression Omnibus (GEO) database of the National Center for Biotechnology Information (NCBI) (https://www.ncbi.nlm.nih.gov/geo/) for analysis. Specifically, GSE227651 contains single-cell sequencing data from the ipsilateral brain hemispheres of mice in the sham group and at 1, 3, and 7 days after transient middle cerebral artery occlusion (tMCAO). GSE104036 includes high-throughput sequencing results of cortical tissues at 3, 6, 12, and 24 h after ischemia-reperfusion in mice. GSE116878 provides mRNA sequencing data from the ipsilateral brain tissues of mice at 3, 12, 24, and 72 h following ischemic stroke. GSE249957 comprises high-throughput sequencing data from BV2 microglia under the oxygen-glucose deprivation/reoxygenation (OGD/R) model and control conditions. GSE22255 contains microarray data of peripheral blood mononuclear cells (PBMCs) from 20 ischemic stroke patients and age- and sex-matched controls.

Single-cell sequencing data analysis

Single-nucleus sequencing data were analyzed using Seurat (version 5.1.0)[31] and Harmony (version 1.2.1)[32], with results visualized using ggplot2 (version 3.5.1) and pheatmap (version 1.0.12). Marker genes for each cell subset were identified using the "FindAllMarkers" function, while differentially expressed genes (DEGs) between groups were determined using the "FindMarkers" function. Enrichment analyses were performed using clusterProfiler (version 4.12.0)[33]. Gene set scoring was conducted with the "AddModuleScore" function. Trajectory analysis of snRNA-seq data was performed using monocle2 (version 2.32.0)[34], and CytoTRACE[35] (version 0.3.3) was applied to determine the trajectory origin.

Transcriptome sequencing data analysis

Data preprocessing was performed using tidyverse (version 2.0.0). Differential expression analysis of transcriptome sequencing data was conducted with DESeq2 (version 1.44.0)[36], while Mfuzz (version 2.64.0) was utilized to reveal dynamic gene expression patterns across time series. Differential analysis of microarray data was performed using the limma package (version 3.60.2)[37]. Gene Ontology (GO)[38] and Kyoto Encyclopedia of Genes and Genomes (KEGG)[39] enrichment analyses were performed using clusterProfiler (version 4.12.0), and gene set scoring was carried out with GSVA (version 1.52.3). Results were visualized using ggplot2 (version 3.5.1) and ClusterGVis (version 0.1.1). The transcription factor activity at different time points post-MCAO was scored using the decoupleR package (version 2.10.0).

Animal experiments

This study was conducted in accordance with the ARRIVE guidelines (Animal Research: Reporting of In Vivo Experiments). C57BL/6 mice (male, 2 months old, 20–22 g) were purchased from the Experimental Animal Center of Nanjing Medical University and housed in the university's animal core facility under a standard 12-h

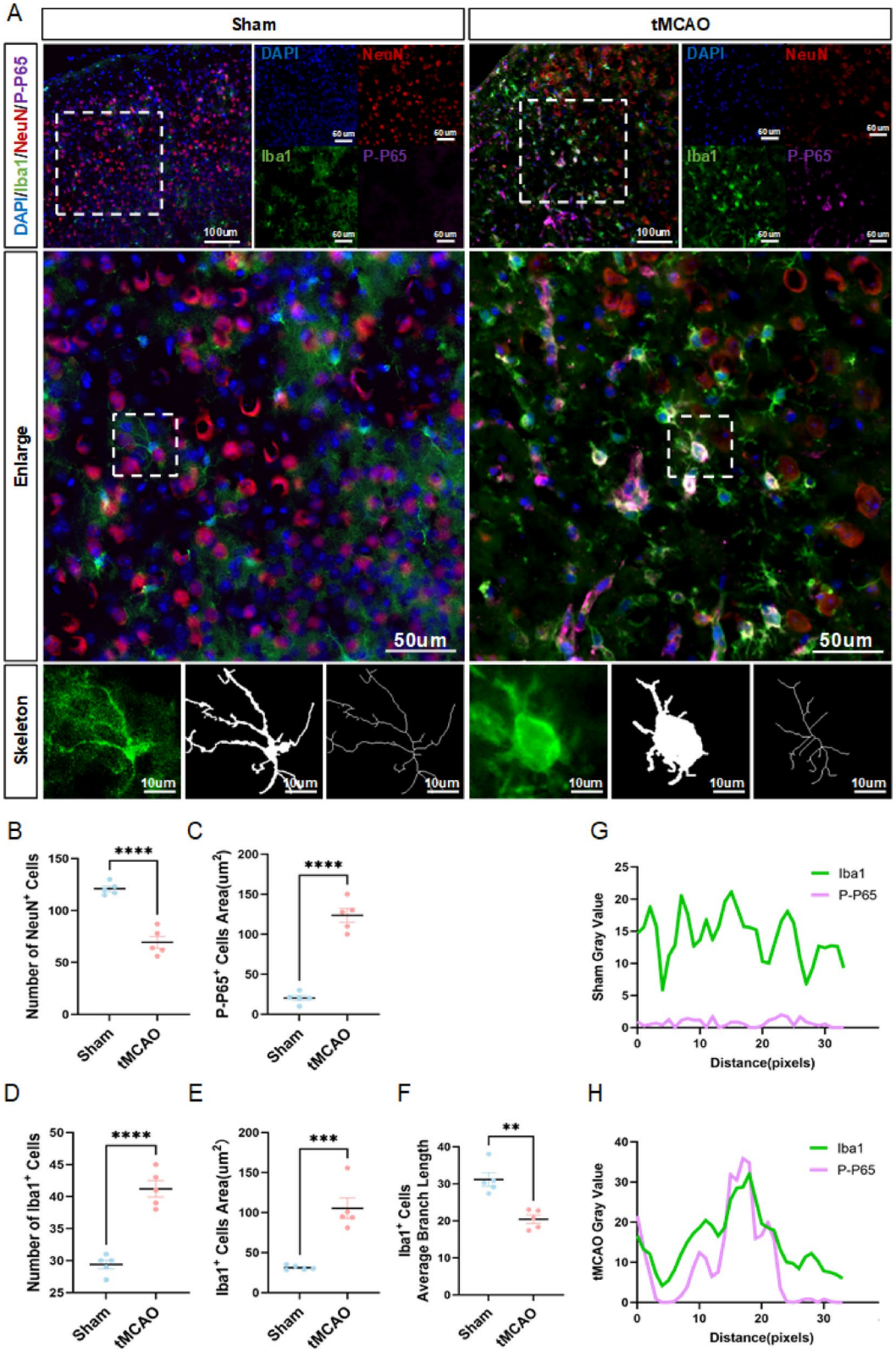

Fig. 7. The activation of microglia in the infarction area of tMCAO mice was increased, accompanied by the phosphorylation of P65. (**A**) Representative images of NeuN, IBA1 and P-P65 fluorescent staining in mouse cortical infarct areas. Skeletal analysis of microglia. (**B**) Statistical analysis of the number of NeuN + cells ($n = 5$). (**C**) Statistical analysis of the area of P-P65 + cells ($n = 5$). (**D**–**F**) Statistical analysis of the number, cell body area, and average branch length of IBA1 + cells ($n = 5$). (**G**–**H**) Quantification of immunofluorescence was conducted to assess the colocalization of IBA1 and P-P65.Data are Mean ± SEM. $*p < 0.05$, $**p < 0.01$, $***p < 0.001$, and $****p < 0.0001$.

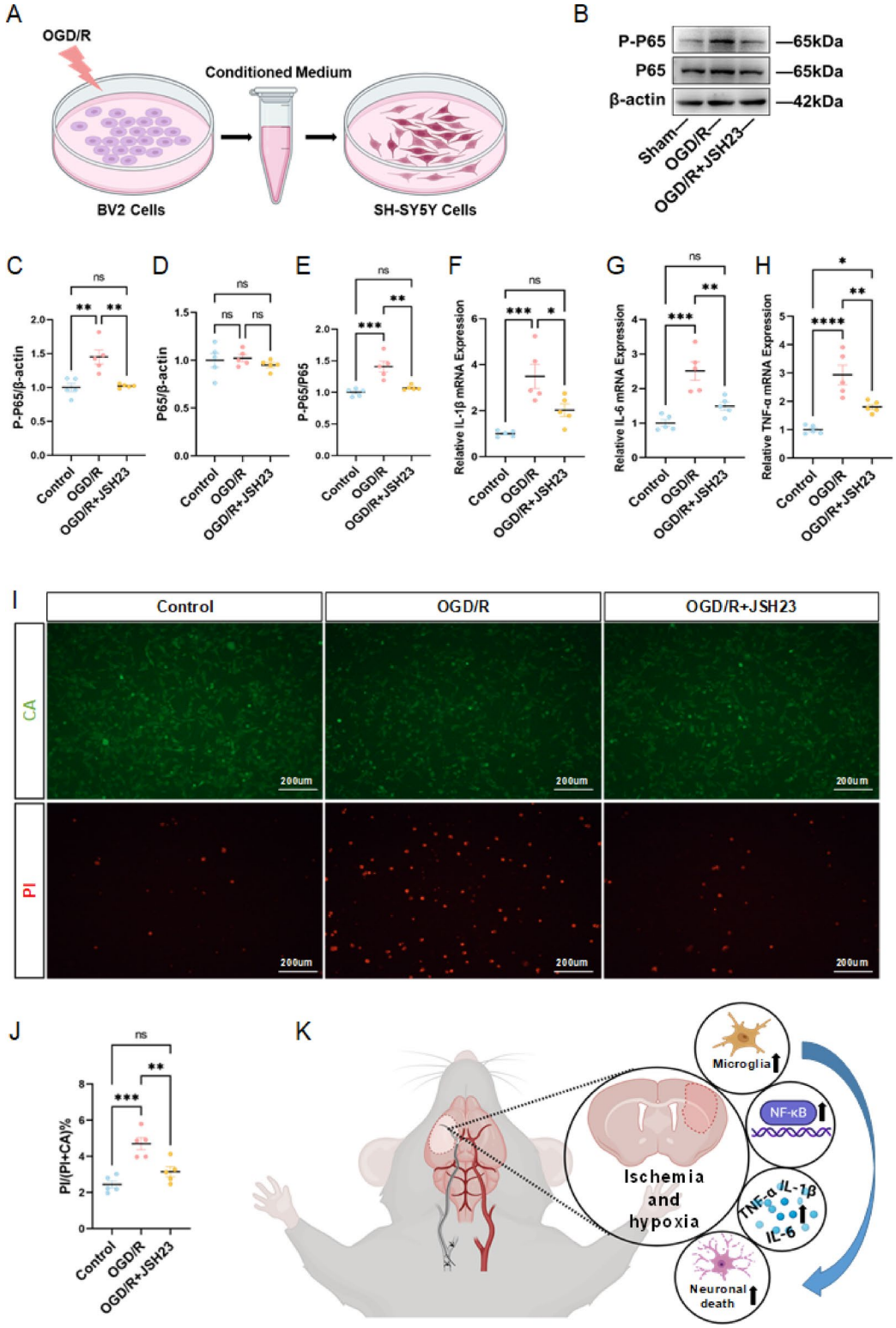

Fig. 8. Inhibition of P65 phosphorylation can reduce the levels of inflammatory factors in microglia (**A**) Schematic diagram of the cell experiments. (**B**–**E**) Representative bands of Western blot and statistical analysis for P-P65, P65, and β-actin ($n = 5$). (**F**–**H**) qPCR statistical analysis of IL-1β, IL-6 and TNF-α ($n = 5$). (**I**,**J**) Proportion of dead cells in SH-SY5Y cells. (**K**) Mechanistic diagram of increased microglial inflammation leading to increased neuronal death in stroke. Data are Mean ± SEM. $*p < 0.05$, $**p < 0.01$, $***p < 0.001$, and $****p < 0.0001$.

light/dark cycle with free access to food and water. All animal experiments were conducted in accordance with the ethical policies and procedures approved by the Animal Welfare and Ethics Committee of Nanjing Medical University (Approval No.: IACUC-2411055). The handling of animals adhered to the principles outlined in the Procedures and Guidelines for Animal Ethics of the People's Republic of China and the Animal Welfare Act. Mice were randomly assigned using a random number table into the Sham group ($n = 13$) and the t-MCAO group ($n = 13$). After a one-week acclimatization period, mice in the t-MCAO group underwent transient middle cerebral artery occlusion (t-MCAO) surgery, while those in the Sham group underwent the same procedure except for vascular ligation and insertion of the filament. Neurological function and cerebral blood flow were assessed 23 h after surgery, followed by euthanasia using CO_2 and tissue collection 24 h after surgery.

Establishment of the ischemia/reperfusion (I/R) brain injury model in mice

A transient middle cerebral artery occlusion (t-MCAO) procedure was performed to induce an I/R brain injury model[40]. Briefly, male C57BL/6J mice were anesthetized with isoflurane and placed on a thermostatic blanket to maintain body temperature. A nylon filament (0.18 ± 0.01 mm, Guangzhou Jialing Biotechnology, Cat#L1800) was inserted into the internal carotid artery (ICA) via the external carotid artery (ECA) and advanced to the middle cerebral artery. Occlusion was maintained for 60 min, after which the filament was removed to restore blood flow to the MCA territory. Sham-operated mice underwent the same surgical procedures without filament insertion.

Cell culture and treatment

BV2 microglial cells and human neuroblastoma SH-SY5Y cells were cultured in DMEM (Cat#C11995500BT, Gibco, USA) supplemented with 10% fetal bovine serum (FBS), 100 U/mL penicillin, and 100 µg/mL streptomycin in a humidified environment of 37 °C, 95% air, and 5% CO_2. BV2 cells were divided into three groups: control (CON), oxygen-glucose deprivation/reoxygenation (OGD/R), and OGD/R + JSH23 (CAT#749886-87-1, MCE, USA) groups[41]. BV2 cells at appropriate density underwent OGD treatment.

Oxygen-glucose deprivation (OGD): The complete medium was replaced with glucose-free DMEM (Life Technologies, Cat#11966-025, Gaithersburg, MD, USA), and BV2 cells were placed in anaerobic bags (Mitsubishi, Japan) along with anaerobic gas packs (Mitsubishi, Japan) to create an environment of 37 °C, 95% N_2, and 5% CO_2. The sealed bags were incubated at 37 °C for 4 h[42].

Reoxygenation with glucose: After 4 h, the anaerobic bags were opened, the glucose-free DMEM was replaced with DMEM containing 10% FBS, and the BV2 cells were incubated at 37 °C, 95% air, and 5% CO_2 for 24 h. BV2 cells from all three groups were collected for Western blot and qPCR experiments. Conditioned media (CM) from the three groups were added to SH-SY5Y cells for co-culture, and cell viability was assessed after 24 h.

Neurological function evaluation

Neurological function was assessed by observing mice behavior and scoring neurological deficits:0: No deficits, normal behavior; 1: Incomplete extension of the contralateral forelimb; 2: Circling behavior (towards the affected side); 3: Loss of voluntary movement but able to stand; 4: No voluntary activity, unconsciousness, or severe paralysis.

The Beam Walk Test was used to assess motor coordination and balance. A 6-mm wide, 50-cm long beam with a safety platform at the end was used. Walking time, error frequency (e.g., paw slips), and success in reaching the platform were recorded. Scoring:0: Normal, no slips; 1: Mild slips, but reached the platform; 2: Multiple slips, but reached the platform; 3: Unable to reach the platform, falls, or circles.The assessments were conducted by a blinded researcher within 23 h after t-MCAO.

Measurement of cerebral blood flow

Cerebral blood flow was measured using a moorFLPI laser speckle flow imager. The skin over the cranial area was retracted, and the skull was exposed while the mouse was placed on a heated pad (37 °C). A charge-coupled device (CCD) camera captured perfusion images under 775 nm laser illumination with an exposure time of 2 ms. Perfusion was displayed as pseudo-color images, ranging from blue (low perfusion) to red (high perfusion), and analyzed using moorFLPI-2 software[43].

Infarct volume measurement

Brain infarct volume was measured using 2,3,5-triphenyltetrazolium chloride (TTC) staining. Each brain was sectioned into five 1-mm slices, incubated with 2% TTC at 37 °C for 10 min, and fixed in 4% paraformaldehyde for 30 min. Infarct volume was calculated as described previously[44].

Immunofluorescence

Brain sections were washed with PBS, and endogenous peroxidase activity was removed with 3% H_2O_2. After blocking for 1.5 h, primary antibodies were added and incubated at 4 °C for 24 h. After washing, secondary antibodies and fluorescent dyes were applied at room temperature for 1.5 h. Nuclei were stained with DAPI. Primary antibodies included anti-NEUN (1:50, Millipore, MAB377), anti-IBA1 (1:500, CST, 17198), and anti-p-P65 (1:800, Millipore, MAB360). The ratio of dead and alive BV2 cells was quantified by (Calcein AM, PI) (Proteintech, PF00007)double fluorescence staining kit. Images were captured using a Nikon fluorescence microscope and analyzed with ImageJ software.

Western blot

Total protein was extracted from brain tissue or BV2 cells using RIPA lysis buffer containing PMSF and phosphatase inhibitors. After centrifugation at 12,000 rpm for 15 min at 4 °C, the supernatant was collected, quantified by the

BCA assay, and boiled with sample buffer at 95 °C for 10 min. Proteins were separated via 8–15% SDS-PAGE, transferred to PVDF membranes, and blocked with 5% skim milk for 1 h at room temperature. Membranes were incubated overnight at 4 °C with primary antibodies, including anti-p-P65 (1:1000, CST), anti-P65 (1:1000, CST), and anti-β-actin (1:2000, Proteintech). HRP-conjugated secondary antibodies (anti-mouse or anti-rabbit, 1:5000, Proteintech) were applied for 1 h at room temperature. Protein bands were visualized using an ECL kit and the Tanon 5200 imaging system, and grayscale intensity was analyzed with ImageJ software.

Quantitative PCR (qPCR)

Total RNA was extracted from the infarct regions of mice or BV2 cells using a total RNA extraction kit (Cat#R401-01, Vazyme, Nanjing, Jiangsu, China), and reverse transcribed into cDNA. qPCR was performed using ChamQ SYBR qPCR premix (Cat#Q341-02, Vazyme), and data were analyzed using the $2^{-\Delta\Delta Ct}$ method. Primer sequences are listed in Supplementary Table S1.

Statistical analysis

Statistical analyses were performed using R (version 4.4.2, http://www.r-project.org) and GraphPad (version 10.0.0). One-way analysis of variance (ANOVA) was used for comparisons among multiple groups, while Student's *t*-test was applied for comparisons between two groups. Additionally, Pearson correlation analysis was conducted to evaluate the relationship between genes and groups. A P-value < 0.05 was considered statistically significant.

Data availability

The single-cell RNA sequencing (scRNA-seq) and bulk RNA-seq datasets analyzed in this study are publicly available through the Gene Expression Omnibus (GEO) repository with accession numbers GSE227651, GSE104036, GSE116878, GSE249957, and GSE22255. All raw data were acquired from previously published studies in accordance with respective data usage agreements.

Received: 9 February 2025; Accepted: 29 April 2025
Published online: 22 May 2025

References

1. Tuo, Q. Z., Zhang, S. T. & Lei, P. Mechanisms of neuronal cell death in ischemic stroke and their therapeutic implications. *Med. Res. Rev.* **42**, 259–305 (2022).
2. Zhang, M. et al. Ischemia-reperfusion injury: Molecular mechanisms and therapeutic targets. *Signal. Transduct. Target. Therapy.* **9**, 12 (2024).
3. Bonev, B. et al. Opportunities and challenges of single-cell and spatially resolved genomics methods for neuroscience discovery. *Nat. Neurosci.* **27**, 2292–2309 (2024).
4. Nayak, D., Roth, T. L. & McGavern, D. B. Microglia development and function. *Annu. Rev. Immunol.* **32**, 367–402 (2014).
5. Dos Santos, I. R. C., Dias, M. N. C. & Gomes-Leal, W. Microglial activation and adult neurogenesis after brain stroke. *Neural Regener. Res.* **16**, 456–459 (2021).
6. Bai, Q., Xue, M. & Yong, V. W. Microglia and macrophage phenotypes in intracerebral haemorrhage injury: Therapeutic opportunities. *Brain* **143**, 1297–1314 (2020).
7. Liu, Y., Wu, L., Peng, W. & Mao, X. Glial polarization in neurological diseases: Molecular mechanisms and therapeutic opportunities. *Ageing Res. Rev.* **104**, 102638 (2024).
8. Wang, N. et al. Machine learning enables discovery of Gentianine targeting TLR4/NF-κB pathway to repair ischemic stroke injury. *Pharmacol. Res.* **173**, 105913 (2021).
9. Mota, M. et al. Neuroprotective epi-drugs quench the inflammatory response and microglial/macrophage activation in a mouse model of permanent brain ischemia. *J. Neuroinflam.*. **17**, 361 (2020).
10. Iadecola, C. & Anrather, J. Stroke research at a crossroad: Asking the brain for directions. *Nat. Neurosci.* **14**, 1363–1368 (2011).
11. Ge, P. et al. TMAO promotes NLRP3 inflammasome activation of microglia aggravating neurological injury in ischemic stroke through FTO/IGF2BP2. *J. Inflamm. Res.* **16**, 3699–3714 (2023).
12. Han, B. et al. Microglial PGC-1α protects against ischemic brain injury by suppressing neuroinflammation. *Genome Med.* **13**, 47 (2021).
13. Zhang, J. et al. Proteomics and transcriptome reveal the key transcription factors mediating the protection of Panax Notoginseng saponins (PNS) against cerebral ischemia/reperfusion injury. *Phytomedicine* **92**, 153613 (2021).
14. He, C., Wang, T., Han, Y., Zuo, C. & Wang, G. E3 ubiquitin ligase COP1 confers neuroprotection in cerebral ischemia/reperfusion injury via regulation of transcription factor C/EBPβ in microglia. *Int. J. Biol. Macromol.* **222**, 1789–1800 (2022).
15. Xu, G. et al. The role and therapeutic potential of nuclear factor KB (NF-κB) in ischemic stroke. *Biomed. Pharmacother.* **171**, 116140 (2024).
16. Wang, H., Yang, Y., Liu, J. & Qian, L. Direct cell reprogramming: Approaches, mechanisms and progress. *Nat. Rev. Mol. Cell. Biol.* **22**, 410–424 (2021).
17. Tian, X. et al. Multi-omics profiling identifies microglial Annexin A2 as a key mediator of NF-κB pro-inflammatory signaling in ischemic reperfusion injury. *Mol. Cell. Proteom.* **23**, 100723 (2024).
18. Kumari, S. et al. The impact of cytokines in neuroinflammation-mediated stroke. *Cytokine Growth Factor. Rev.* **78**, 105–119 (2024).
19. Candelario-Jalil, E., Dijkhuizen, R. M. & Magnus, T. Neuroinflammation, stroke, blood-brain barrier dysfunction, and imaging modalities. *Stroke* **53**, 1473–1486 (2022).
20. Xu, J. et al. Loureirin C ameliorates ischemia and reperfusion injury in rats by inhibiting the activation of the TLR4/NF-κB pathway and promoting TLR4 degradation. *Phytother Res.* **36**, 4527–4541 (2022).
21. Cai, J. et al. Cyclo-(Phe-Tyr) as a novel Cyclic dipeptide compound alleviates ischemic/reperfusion brain injury via JUNB/JNK/NF-κB and SOX5/PI3K/AKT pathways. *Pharmacol. Res.* **180**, 106230 (2022).
22. Ganbold, T., Bao, Q., Zandan, J., Hasi, A. & Baigude, H. Modulation of microglia polarization through Silencing of NF-κB p65 by functionalized curdlan Nanoparticle-Mediated RNAi. *ACS Appl. Mater. Interfaces.* **12**, 11363–11374 (2020).
23. Gong, P. et al. Downregulation of Nogo-B ameliorates cerebral ischemia/reperfusion injury in mice through regulating microglia polarization via TLR4/NF-kappaB pathway. *Neurochem Int.* **167**, 105553 (2023).
24. Yang, C. et al. Analgecine regulates microglia polarization in ischemic stroke by inhibiting NF-κB through the TLR4 MyD88 pathway. *Int. Immunopharmacol.* **99**, 107930 (2021).

25. Preconditioned extracellular vesicles from hypoxic. microglia reduce poststroke AQP4 depolarization, disturbed cerebrospinal fluid flow, astrogliosis, and neuroinflammation - PubMed. https://pubmed.ncbi.nlm.nih.gov/37554272/
26. He, T. et al. Sestrin2 regulates microglia polarization through mTOR-mediated autophagic flux to attenuate inflammation during experimental brain ischemia. *J. Neuroinflam.*. **17**, 329 (2020).
27. Zeng, F. et al. Single-cell analyses reveal the dynamic functions of Itgb2 + microglia subclusters at different stages of cerebral ischemia-reperfusion injury in transient middle cerebral occlusion mice model. *Front. Immunol.* **14**, 1114663 (2023).
28. Kim, J. et al. Transcriptome analysis reveals intermittent fasting-induced genetic changes in ischemic stroke. *Hum. Mol. Genet.* **27**, 1497–1513 (2018).
29. Bu, J. et al. RNA sequencing analyses reveal the potential Anti-Inflammatory mechanisms of Acacetin against ODG/R injuries in microglia. *J. Inflamm. Res.* **17**, 3641–3652 (2024).
30. Krug, T. et al. TTC7B emerges as a novel risk factor for ischemic stroke through the convergence of several genome-wide approaches. *J. Cereb. Blood Flow. Metab.* **32**, 1061–1072 (2012).
31. Hao, Y. et al. Dictionary learning for integrative, multimodal and scalable single-cell analysis. *Nat. Biotechnol.* **42**, 293–304 (2024).
32. Korsunsky, I. et al. Fast, sensitive and accurate integration of single-cell data with harmony. *Nat. Methods*. **16**, 1289–1296 (2019).
33. Wu, T. et al. ClusterProfiler 4.0: A universal enrichment tool for interpreting omics data. *Innov. (Camb)*. **2**, 100141 (2021).
34. Qiu, X. et al. Single-cell mRNA quantification and differential analysis with census. *Nat. Methods*. **14**, 309–315 (2017).
35. Gulati, G. S. et al. Single-cell transcriptional diversity is a hallmark of developmental potential. *Science* **367**, 405–411 (2020).
36. Love, M. I., Huber, W. & Anders, S. Moderated estimation of fold change and dispersion for RNA-seq data with DESeq2. *Genome Biol.* **15**, 1–21 (2014).
37. Ritchie, M. E. et al. Limma powers differential expression analyses for RNA-sequencing and microarray studies. *Nucleic Acids Res.* **43**, e47 (2015).
38. Gene Ontology Consortium. Gene ontology consortium: Going forward. *Nucleic Acids Res.* **43**, D1049–1056 (2015).
39. Kanehisa, M. & Goto, S. KEGG: Kyoto encyclopedia of genes and genomes. *Nucleic Acids Res.* **28**, 27–30 (2000).
40. Cai, W. et al. FOXP3 + macrophage represses acute ischemic stroke-induced neural inflammation. *Autophagy* **19**, 1144–1163 (2023).
41. Chen, S. et al. RelA/p65 Inhibition prevents tendon adhesion by modulating inflammation, cell proliferation, and apoptosis. *Cell. Death Dis.* **8**, e2710 (2017).
42. Zhu, M. et al. Na+/K+-ATPase-dependent autophagy protects brain against ischemic injury. *Signal. Transduct. Target. Ther.* **5**, 55 (2020).
43. Guo, R. B. et al. Iptakalim improves cerebral microcirculation in mice after ischemic stroke by inhibiting pericyte contraction. *Acta Pharmacol. Sin.* **43**, 1349–1359 (2022).
44. Qian, Y. et al. SRGN amplifies microglia-mediated neuroinflammation and exacerbates ischemic brain injury. *J. Neuroinflam.*. **21**, 35 (2024).

Acknowledgements

We thank the researchers of GSE227651, GSE104036, GSE116878, GSE249957, and GSE22255 for sharing data online.

Author contributions

All authors made a significant contribution to the work reported, whether that is in the conception, study design, execution, acquisition of data, analysis and interpretation, or in all these areas; took part in drafting, revising or critically reviewing the article; gave final approval of the version to be published; have agreed on the journal to which the article has been submitted; and agree to be accountable for all aspects of the work.

Funding

The study was supported by the Excellent Postdoctoral Program of Jiangsu Province (Grant Number 2023ZB023).

Declarations

Competing interests

The authors declare no competing interests.

Ethics statement

This study was conducted in accordance with the ARRIVE guidelines (Animal Research: Reporting of In Vivo Experiments). All animal experiments were conducted in accordance with the ethical policies and procedures approved by the Animal Welfare and Ethics Committee of Nanjing Medical University (Approval No: IACUC-2411055).

Additional information

Supplementary Information The online version contains supplementary material available at https://doi.org/10.1038/s41598-025-00524-2.

Correspondence and requests for materials should be addressed to Y.G., T.W. or B.S.